HHS Public Access

Author manuscript

Biochemistry. Author manuscript; available in PMC 2019 July 25.

Published in final edited form as:

Biochemistry. 2018 July 31; 57(30): 4395–4403. doi:10.1021/acs.biochem.8b00349.

NMR Solution Structure of the Recombinant Fragment Containing Three Fibrin-Binding CR Domains of the Very Low Density Lipoprotein Receptor

Koyeli Banerjee[†], **Sergiy Yakovlev**[‡], **James M. Gruschus**[†], **Leonid Medved**[‡,*], **Nico Tjandra**[†,*]

[†]Laboratory of Molecular Biophysics, National Heart, Lung, and Blood Institute, National Institutes of Health, Bethesda, Maryland 20892, United States

[‡]Center for Vascular and Inflammatory Diseases and Department of Biochemistry and Molecular Biology, University of Maryland School of Medicine, Baltimore, Maryland 21201, United States

Abstract

Our previous studies revealed that interaction of fibrin with the very low density lipoprotein (VLDL) receptor plays a prominent role in transendothelial migration of leukocytes and thereby inflammation. The major goal of our subsequent studies is to establish the structural basis for this interaction. As the first step toward this goal, we localized the fibrin-binding sites within cysteine-rich (CR) domains 2–4 of the VLDL receptor. In the present study, we have made a next step toward this goal by establishing NMR solution structure of the recombinant VLDLR(2–4) fragment containing all three fibrin-binding CR domains of this receptor. The structure revealed that all three CR domains have similar general fold. Each domain contains a calcium-binding loop and the loop in CR3 domain has a unique conformation relative to the other two. The domains CR2 and CR3 interact with each other while CR4 is flexible relative to the other two domains. Further, analysis of the electrostatic potential surface of VLDLR(2–4) revealed extended negatively charged regions in each of its CR domains. The presence of these regions suggests that they may interact with three positively charged clusters of fibrin βN-domain whose involvement in interaction with the VLDL receptor was demonstrated earlier. Altogether, these findings provide a solid background for our next step towards establishing the structural basis for fibrin-VLDL receptor interaction.

Graphical Abstract

[*]**To whom correspondence should be addressed.:** N.T.: tjandran@nhlbi.nih.gov; phone: (301) 402-3029; fax: (301) 402-3405. L.M.: lmedved@som.umaryland.edu; phone: (410) 706-8065; fax: (410) 706-8121.

The authors declare no competing financial interest.

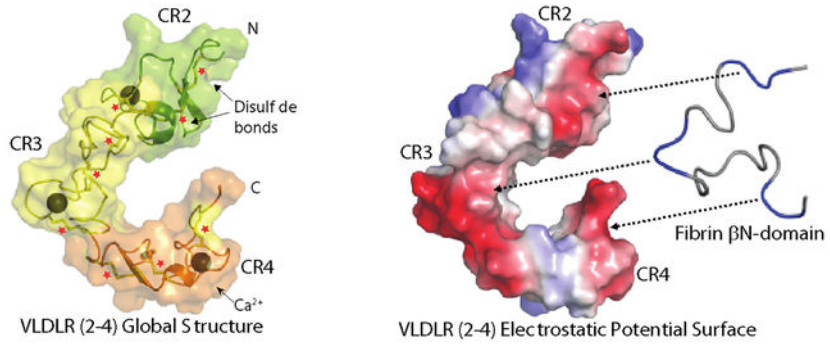

The very low density lipoprotein receptor (VLDLR) is a member of the low density lipoprotein (LDL) receptor family, which includes LDL receptor, LRP, and several other multifunctional cellular receptors.[1] A common feature of these receptors is that they all have modular domain structure,[1] i.e. each of them contains a number of various homologous sequences (modules) that are folded into compact structures (domains). The N-terminal portion of the VLDL receptor consists of a cluster of eight cysteine-rich complement-type repeats (modules) called CR domains followed by three EGF-like domains and β-propeller domain, O-linked sugar domain, and transmembrane and cytoplasmic domains.[1,2] CR domains of VLDLR and other LDL receptor family members are also commonly referred to as ligand-binding repeats or domains since most of the ligands for these receptors bind to them. Each CR domain consists of approximately 40 amino acid residues including six Cys that form three intra-domain disulfide bonds. Numerous structural studies of CR domains from different LDL receptor family members revealed that they have similar basic three-dimensional folds and the structure of each CR domain is stabilized by the disulfide bonds and Ca^{2+} ion[3]. At the same time, the ligand-binding specificity of various CR domains in many cases is different[1, 4] suggesting that the structure of their ligand-binding sites is not the same.

VLDLR is a multifunctional receptor found in different tissues including vascular endothelium.[2,5] Originally, VLDLR was proposed to function as a peripheral lipoprotein receptor involved in the binding and delivery of triglyceride-rich lipoproteins into peripheral fatty acid active tissues.[6] This function was later confirmed in the *in vivo* experiments.[7, 8] It was also shown that this receptor interacts with reelin,[9] RAP,[10] thrombospondin-1,[11] hepatitis C virus[12] and human rhinovirus HRV2,[13] and several proteinase-serpin complexes.[14–16] These interactions play an important role in endocytosis of variety of ligands, reelin signaling and neuronal migration, viral infections, angiogenesis, and tumor growth.[5,17–19] More recently, we found that the VLDL receptor also interacts with fibrin, whose major function is to form fibrin clots that seal damaged vasculature and prevent blood leaking, and this interaction promotes transendothelial migration of leukocytes and thereby inflammation.[20] We also found that inhibition of this interaction with the specific anti-VLDLR monoclonal antibodies significantly reduces leukocyte transmigration in the *in vitro* assay.[21] Further, our experiments revealed that such antibodies exhibit prominent anti-inflammatory properties and significantly reduce myocardial injury induced by ischemia-reperfusion in the *in vivo* models.[21]

Taking into account the significant role of fibrin-VLDLR interaction in fibrin-dependent inflammation, we focused our subsequent studies on the establishment of its molecular mechanism. First, we localized the VLDLR-binding site to a pair of fibrin βN-domains, each formed by fibrin β chain residues 15–64, and found that a recombinant $(\beta 15–66)_2$ fragment corresponding to these domains has the same high affinity to VLDLR as fibrin.[20] Second, we localized the complementary fibrin-binding site to CR domains 2–4 of the VLDL receptor by preparing recombinant fragments containing various combination of its CR domains and testing their interaction with the VLDLR-binding domains of fibrin.[22] We also found that among these fragments, the recombinant VLDLR(2–4) fragment containing CR domains 2–4 had practically the same high affinity to fibrin as the entire extracellular portion of the VLDL receptor or its VLDLR(1–8) fragment containing all eight ligand-binding CR domains.[22] This finding suggests that all three CR domains of VLDLR(2–4) preserve their native conformation and fibrin-binding properties of the entire VLDL receptor. The major objective of the present study was to establish NMR solution structure of the fibrin-binding VLDLR(2–4) fragment, which is important for establishing the structural basis for fibrin-VLDLR interaction.

MATERIALS AND METHODS

Preparation of the Recombinant VLDLR(2–4) Fragment.

^{15}N- or $^{15}N/^{13}C$-labeled recombinant human VLDLR(2–4) fragment consisting of CR domains 2–4 (amino acid residues Lys^{42}–Pro^{163}) and tagged with six His residues at the C-terminus was expressed in *E. coli* in minimal media supplemented with either $^{15}NH_4Cl$ or $^{15}NH_4Cl$ and $^{13}C_6$-glucose, respectively, and subsequently purified and refolded as described previously for non-labeled VLDLR(2–4).[22] After refolding, the labeled VLDLR(2–4) fragment was isolated on RAP-Sepharose and subsequently fractionated on a Superdex-75 column in 20 mM Tris buffer, pH 7.4, containing 150 mM NaCl, 2 mM $CaCl_2$, 0.1 mM PMSF, and 0.02% NaN_3 to separate its monomeric fraction. The purity and folding status of the monomeric VLDLR(2–4) fragment were confirmed by SDS-PAGE and fluorescence spectroscopy, respectively, as we described earlier.[22]

NMR Data Collection.

The purified VLDLR(2–4) fragment was screened for better solubility, pH, salt concentration, and temperature using NMR by monitoring its HSQC spectra quality. The buffer conditions for VLDLR(2–4) were changed to get maximum peak resolution and minimum peak width in $^{15}N,^{1}H$ HSQC. The best buffer conditions were found to be 50 mM sodium acetate, pH 6.2, with 100 mM NaCl, 2 mM $CaCl_2$, and 0.1 mM PMSF. All NMR experiments were performed at 306.5 K on Bruker Avance 600 MHz or Bruker Avance 800 MHz spectrometers with cryogenic probes. The experiments used for backbone resonance assignments were 3-dimensional HNCACB[23], CBCA(CO)NH[24], HNCA[25], and HNCO[26]. ^{13}C-edited NOESY-HSQC[27] and MQ-HCCH-TOCSY[28] experiments were performed for the side-chain chemical shift assignments. The MQ-HCCH-TOCSY was utilized to assign the ^{1}H and ^{13}C resonances of the methyl groups using uniformly ^{13}C-labeled samples. For assignment of intramolecular NOE distance restraints, 3-dimensional ^{15}N-edited NOESY-HSQC[29], 3-dimensional ^{13}C-edited NOESY-HSQC[27], and 4-dimensional $^{13}C/^{13}C$-edited

NOESY[30] experiments were performed. All NOESY experiments were acquired with 92 ms mixing time (τ_m). All NMR data were processed using NMRPipe and analyzed using NMRDraw[31], CCPN Analysis 2.4.2[32], and PIPP[33]. All NMR protein samples were within 250–300 μM concentrations.

Backbone ^{15}N Relaxation Measurements.

The ^{15}N T_1 backbone relaxation dynamics measurements were done at 800 MHz proton resonance frequency with 2048 × 256 complex points along the t1 and t2 dimensions. The inversion recovery delays for T_1 measurements were 8, 120, 320, 600, 880, 1200, 1600, and 2240 ms. The ^{15}N $T_{1\rho}$ measurements were performed under the same acquisition parameters with relaxation delays of 1, 10, 20, 35, 45, 60, 70, and 85 ms. Error for the correlation time was estimated by randomly removing 10% of the data and refitting. This process was repeated 20 times.

Residual Dipolar Coupling Measurements.

Residual dipolar couplings (RDCs) is one of the useful tools which can be used for protein structure determination and refinement.[34, 35] RDCs of the backbone amide were measured in the absence or presence of alignment medium containing 10 mg/mL of Pf1 filamentous phage (Asia Biotech) to the double labeled ^{13}C/^{15}N-VLDLR(2–4) fragment in H_2O. The 2D ^{1}H-^{15}N HSQC spectra of both VLDLR(2–4) with and without Pf1 phage showed no obvious chemical shift changes indicating the alignment medium did not affect the global conformation of VLDLR(2–4). The Pf1 concentration in the sample was confirmed by ^2H_2O splitting at 14.6 Hz[36]. Two IPAP experiments[37] were performed on two samples of VLDLR(2–4), with and without Pf1 phage, to obtain the isotropic and anisotropic J_{NH} values, respectively. The RDCs (D_{NH}) were calculated by subtracting the isotropic J_{NH} from the anisotropic values.

Structure Calculation.

The ^{15}N NOESY and 4-dimensional ^{13}C/^{13}C-edited NOESY cross-peaks were identified and assigned. The corresponding peak intensities were translated into ^{1}H-^{1}H distances. Hydrogen bond restraints were derived from the VLDLR homologous structure (PDB: 1LDL). VLDLR(2–4) backbone dihedral angle restraints ϕ and ψ were calculated from the backbone chemical shifts using TALOS-N[38]. The structure of VLDLR(2–4) was calculated using simulated annealing protocol in the Xplor-NIH[39, 40]. The calculation employed 1606 NOE, 106×2 ϕ and ψ dihedral angle restraints. Distance restraints between each Ca^{2+} ion and its corresponding six liganded oxygen atoms were included (2.4 Å), and the final refinement also employed 9×2 hydrogen bond restraints in regions of confirmed secondary structure. In addition, a total of 104 D_{NH} restraints were used in the structure calculation. The D_{NH} were grouped into three classes. The first class belongs to the CR2–3, while the second goes with CR4. D_{NH} for residues in flexible loops are grouped into the third class. Each class was treated independently, thus having their own alignment tensor in the calculation. The D_{NH} in the first two classes were restrained using harmonic potential, while the third class was restrained using half open square potential. All the structure figures are prepared using PyMOL (The PyMOL Molecular Graphics System, Version 1.8 Schrödinger, LLC.) except Figure 5, which was made in MOLMOL[41].

RESULTS

^{15}N HSQC Spectrum and Resonance Assignment of the VLDLR(2–4) Fragment.

Figure 1 shows a two-dimensional ^{1}H-^{15}N HSQC NMR spectrum of the VLDLR(2–4) fragment comprising CR domains 2–4 obtained at NMR proton frequency of 600 MHz. For the 121-residue fragment, most of the resonances are well resolved. With the analysis of the NMR data, nearly 95% of the backbone resonances were assigned. Among the six His tag residues located at the C-terminus of VLDLR(2–4), only the last C-terminal His was assigned. We observed characteristic large downfield shifts (>1 ppm) of aspartate (D23, D25, D27, D33, D66, D70, D76, D109, D115), glutamate (E34, E68, E77, E116), asparagine (N105), and glycine (G24, G67, G106) residues involved in Ca^{2+} ion coordination. This identification aided backbone assignment as analogous CR domain residues in each calcium-binding site had similar chemical shifts. It should be noted that the residue numbering in the VLDLR(2–4) fragment here and elsewhere is Lys^{1}−Pro^{121}, which corresponds to the original Lys^{42}−Pro^{163} numbering of this fragment in the VLDL receptor.

Secondary Structure of the VLDLR(2–4) Fragment.

The secondary structure of VLDLR(2–4) was determined based on NOE connectivities and the δC_α, δC_β, and chemical shift index (CSI) values. The CSI was calculated from $\delta C_\alpha - \delta C_\beta$. The values of $\delta C\alpha$ and δC_β were obtained as the differences between the experimentally observed $^{13}C_\alpha$ and $^{13}C_\beta$ chemical shifts and the corresponding random coil chemical shifts. Typically, a positive CSI corresponds to α-helical conformation while negative CSI indicates β-sheet structure. A summary of these data is shown in Figure 2. The calculated chemical shift index[42] from the assigned C_α and C_β secondary chemical shifts indicates very small stretches of α-helical or β-sheet structures and mostly loop and random coil structures. In each of the CR domains, the antiparallel β-sheet region forms a β-hairpin structure followed by the Ca^{2+}-binding motif. The repetitions of the secondary structure in the regions 20–34, 64–77, and 102–116 are consistent with the Ca^{2+}-binding region in each of the CR domains.

Relaxation Dynamics Measurements of the VLDLR(2–4) Fragment.

The backbone T_1 and $T_{1\rho}$ of ^{15}N-VLDLR(2–4) were measured at 800 MHz proton resonance frequencies. Figure 3 shows that CR domains 2 and 3 have distinct distribution of their T_1 and $T_{1\rho}$ values compared to CR4. The average T_1 for the CR2 and CR3 were very similar, 0.77 ± 0.03 s, while the average T_1 for CR4 was 0.64 ± 0.03 s. The observed $T_{1\rho}$ values for CR2 and CR3 were 0.058 ± 0.005 s and that for CR4 was 0.083 ± 0.005 s. The similar average relaxation values for CR2 and CR3 suggest that these domains are rather tightly coupled and tumble together. In contrast, the higher average $T_{1\rho}$ value and lower T_1 value for CR4 indicate that the rotational diffusion of this domain is more rapid than that of CR2 or CR3. In fact, calculation of the expected T_1 and $T_{1\rho}$ values using model free spectral densities[43] resulted in an estimated rotational correlation time (τ_c) of 8.24 ± 0.04 ns for CR2 and CR3 and 6.18 ± 0.02 ns for CR4. As a consequence of these observations, some of the structural restraints, in particular the residual dipolar couplings, were adjusted to reflect that CR2 and CR3 constitute one rotationally tumbling unit, while CR4 tumbles separately.

Solution Structure of the VLDLR(2–4) Fragment.

The structure of the VLDLR(2–4) fragment was calculated using NOE-derived distance restraints, generic hydrogen bonds, TALOS-derived dihedral angles, and dipolar coupling restraints (D_{NH}) (see Table 1). Despite having a well resolved ^{15}N HSQC spectrum typical for proteins with well-defined regular secondary and tertiary structures, very few long-range distance restraints (i-j ≥ 5) were observed in the ^{15}N-edited NOESY spectrum, and the majority of long-range restraints came from the 4D ^{13}C-edited NOESY spectrum. The calculated atomic coordinates and restraints, and the chemical shift assignments were deposited to the Protein Data Bank with the following accession codes: PDB ID 6BYV, BMRB ID 30388. The ensemble of 20 lowest energy structures is shown in Figure 4. The superposition of calculated 20 lowest energy structures of the VLDLR(2–4) fragment do not have any distance or dihedral violations exceeding 0.5 Å or 1.5 Å, respectively. The backbone RMSD values of the structured regions of the CR domains are 0.64 Å (residues 5–38), 0.65 Å (residues 43–74), and 1.94 Å (residues 80–98 and 102–116), and the corresponding all-heavy-atom RMSD values are 0.98, 0.95, and 2.07 Å, respectively. The detailed structural statistics for the ensemble of 20 lowest energy structures is provided in Table 1.

The ensemble of the lowest energy structures is consistent with the relaxation data suggesting that CR2 and CR3 domains form one rigid unit, while CR4 is a separate folded domain connected by a flexible linker. When the ensemble is superposed using just CR2 and CR3, the RMSD values for CR4 are 7.50 Å and 7.63 Å for backbone and all heavy atoms, respectively, with the distribution of CR4 positions spreading in a cone with a maximum angle span of 75° ± 15°, as shown in Figure 4A. The structure shows an extended form with CR2 and CR3 domains being packed more closely than CR4. The dynamic flexibility of the loop between CR3 and CR4 is further supported by the high $T_{1\rho}$ values of the linker residues (81–85) (Figure 3).

There are eighteen Cys residues in the VLDLR(2–4) fragment, six in each CR domain. All these Cys form disulfide bonds (Figure 5) which are evident from the large C_β chemical shift values compared to the C_β chemical shift values of reduced Cys residues. Cys 23, 65, and 104 have slightly lower C_β chemical shift values than the others, perhaps due to their proximity to the positively charged Ca^{2+} ion. Since there are no long stretches of regular secondary structures, these disulfide bonds should make significant contribution to the overall stability of the protein. All three CR domains have similar fold and disulfide bond arrangement as shown in Figure 5, consistent with their sequence similarity. Domain CR2 has two short antiparallel β-strands forming a β-hairpin followed by a turn going into the calcium-binding loop. The N-terminal portion of CR2 is connected to the second β-strand by the Cys3-Cys15 disulfide bridge, while the first β-strand is connected to the end of the calcium-binding loop by Cys10-Cys28. The calcium-binding loop is followed by a short helical turn, whose C-terminal end is connected to the middle of the calcium-binding loop by the Cys39-Cys22 disulfide bridge. Domains CR3 and CR4 also have the β-hairpin and follow the same disulfide pattern, except they do not possess the short helical turn near their calcium-binding loops. The disulfide bond formation is conserved in all domains by

alternating Cys residues in the following order: Cys1-Cys3, Cys2-Cys5, and Cys4-Cys6. The β-hairpins in the first two domains, CR2 and CR3, are oriented at an angle close to 90°.

Consistent with the homologous CR domain structure of the LDL receptor[44], Ca^{2+} ions in all three domains are liganded to negatively charged side chains of Asp and Glu residues. Figure 6 shows residues in each CR domain that bind Ca^{2+} ion forming a complete octahedral geometry. In CR2 domain, Ca^{2+} ion coordinates with side chains of D23, D27, D33, E34 and backbone carbonyls of W20 and D25 (Figure 6A). A similar coordination pattern is maintained in CR3 and CR4 domains as well. In CR3, residues D66, D70, D76, and E77 coordinate to Ca^{2+} ion through their side chains, and the backbone carbonyls of W63 and E68 complete the coordination (Figure 6B). The pattern is slightly different in CR4, in which Trp is replaced by Phe and two of the acidic amino acid residues (D23 and D25 in CR2 and D66 and E68 in CR3) are replaced by N105 and Q107 with uncharged side chains (Figure 6D). Therefore, Ca^{2+} coordinates with N105, D109, D115, and E116 through their side chains, and with F102 and Q107 through their backbone carbonyls (Figure 6C). Even though the coordination is very similar in all three CR domains, the structure of the short loop region in them is not the same. One important distinction is the direction of the fold of the calcium-binding loop in CR3 compared to the other two. In the orientation of the calcium-binding loops as shown in Figure 6A–C, the loop immediately following D27 in CR2 or D109 in CR4 towards the N-terminus is lower than the plane formed by Ca^{2+} ion and the last three ligands (D27, D33, and E34 in CR2, and D109, D115, and E116 in CR4). In contrast, the same loop is higher than the corresponding plane in CR3 (formed by Ca^{2+}, D70, D76, and E77). Also notably, the N-terminal portions of the CR2 and CR4 loops are pointing up in the configuration in Figure 6A–C, while the CR3 N-terminal portion is pointing down. Inserts in the sequence of these calcium-binding loops, as highlighted in their sequence alignment (Figure 6D), might contribute to their different conformations.

DISCUSSION

Our previous studies revealed that interaction of fibrin with the VLDL receptor plays a prominent role in transendothelial migration of leukocytes and thereby fibrin-dependent inflammation.[20, 21] However, the molecular mechanism of this interaction and the structural basis for it are still poorly understood. To establish such a mechanism, we first localized complementary binding sites within a pair of fibrin βN-domains and CR domains 2–4 of the VLDL receptor.[20, 22, 45] In the present study, we have taken our next step toward establishing the structural basis for this interaction, namely, we have determined NMR solution structure of the VLDLR(2–4) fragment containing all three fibrin-binding CR domains of the VLDL receptor.

The major challenge in determining the structure of VLDLR(2–4) was the sequence homology between all three CR domains of this fragment and similarity in their overall folds that resulted in signal overlaps and some assignment ambiguities. This is rather typical for extracellular proteins containing multiple repeats of similar domains, such as complement-control proteins that can have up to 30 of such modules,[46] which at most only three modules could be solved by NMR at one time. In VLDLR(2–4), the downfield shifted resonances due to calcium coordination, slight differences in the calcium ligands, plus differences in the

structure of the calcium-binding loops reduced the resonance overlap problems for residues in those regions and facilitated analysis of NMR data.

It should be noted that the X-ray crystal structure of a complex between a fragment containing CR domains 2–3 of the VLDL receptor and the minor group human rhinovirus HRV2 have been previously solved,[13] as well as the X-ray structure of a complex between a fragment containing CR domains 1–3 of VLDLR and HRV2.[47] In both X-ray structures, only one of the CR domains could be observed, at low resolution, and it was assumed that the observed domain corresponded to CR3. In the present study, we solved NMR solution structure of the three fibrin-binding CR domains 2–4 of VLDLR, allowing us to evaluate spatial arrangement of these domains in solution and interaction between them at atomic resolution. We can also test which of the two CR domains of VLDLR(2–4), CR2 or CR3, is common with the X-ray structures, i.e. is closest structurally to the CR domain observable by X-ray. Superposing the observed CR domain in the HRV2-bound structure shows a better fit to CR2 than to CR3 (pairwise RMSD values of 4.9Å vs. 6.2Å). This suggests that perhaps it was CR2, not CR3, that was observed in the X-ray structures. It should be noted that a DALI structural similarity search for the CR domains revealed matches not just to the other known LDL-type receptors, but also to auxiliary domains present in hemoglobin complexes of earthworms (PDB codes 2GTL and 4U8U, species Lumbricus terrestris and Glossoscolex paulistus, respectively). All the same disulfide bonds are present, and Ca^{2+} is bound by negatively charged residues in analogous positions.

The interdomain regions of the VLDLR(2–4) structure were examined for interactions that might explain why CR2 and CR3 tumble together in solution as one unit, whereas CR4 comprises a separately tumbling domain connected by a dynamic, flexible linker. While no obvious salt-bridges or hydrophobic interactions are apparent, CR2 and CR3 have a good number of interdomain contacts as observed through 3D NOESY (or 4D-NOESY). In contrast, much fewer interdomain side chain contacts were observed between CR3 and CR4 domains. Aligning the sequences of the three CR domains to each other, CR2 has a two-residue insertion, residues S35 and P36, at the end of the calcium-binding loop adjacent to the helical turn (Figure 6D). The sequence of CR3 also has a two-residue insertion, but in a different location, residues S55 and T56, in the loop of the β-hairpin. Both these insertions pack against the residues linking CR2 and CR3 (Figure 7), and thus might play some stabilizing role. In contrast, CR4 lacks any insertions, and CR3 lacks the insertion corresponding to that of CR2, which could explain the greater flexibility seen for the linker between CR3 and CR4.

The VLDLR(2–4) fragment has many negatively charged residues in addition to those whose side chains coordinate to the Ca^{2+} ions. The electrostatic surface potential of the VLDLR(2–4) fragment shown in Figure 8A reveals that these residues form extended negatively charged regions in the three CR domains, with the most prominent one in the calcium-binding loop of CR3. Our recent study with fibrin βN-domain mutant fragments revealed that the βN-domains interact with CR domains 2–4 of the VLDL receptor through three clusters of positively charged Arg/Lys residues.[45] Based on this finding and electrostatic potential of VLDLR(2–4), one can speculate that the positively charged side chains of the βN-domain clusters (Figure 8B) bind to these negatively charged regions of CR

domains 2–4 of the VLDL receptor. Further structural studies are required to test this speculation.

In summary, the present study established NMR solution structure of the fibrin-binding region of the VLDL receptor containing CR domains 2–4. The structure revealed that the overall fold of all three CR domains is similar to that of CR domains of other members of the LDL receptor family members, and CR2 and CR3 domains interact with each other forming a rigid elongated structure while CR4 domain is flexible relative to the other two domains. The structure also revealed an extended negatively charged region in each of the three CR domains suggesting that these regions may interact with three positively charged cluster of fibrin βN-domain, which were previously shown to be involved in the interaction with the VLDL receptor.[45] Our previous study identified conditions for formation of a stable complex between the fibrin-binding VLDLR(2–4) fragment of the VLDL receptor and the VLDLR-binding $(\beta 15–66)_2$ fragment representing a pair of fibrin βN-domains.[22] Having established the structure of VLDLR(2–4), we have taken another step towards NMR study of this complex and establishment of the structural basis for fibrin-VLDL receptor interaction.

Funding

This work was supported by the Intramural Research Program of the National Heart, Blood, and Lung Institute to N.T., and by National Institutes of Health Grant HL056051 to L.M.

ABBREVIATIONS

LDL	low density lipoprotein receptor
VLDLR	very low density lipoprotein (VLDL) receptor
VLDLR(2–4)	recombinant fragment of the VLDL receptor containing three fibrin-binding CR domains
PMSF	phenylmethylsulfonyl fluoride
HSQC	heteronuclear single quantum coherence
NOESY	nuclear Overhauser effect spectroscopy
RMSD	root-mean-square-deviation

REFERENCES

(1). Lillis AP, Van Duyn LB, Murphy-Ullrich JE, and Strickland DK (2008) LDL receptor-related protein 1: unique tissue-specific functions revealed by selective gene knockout studies, Physiol. Rev 88, 887–918. [PubMed: 18626063]

(2). Takahashi S, Sakai J, Fujino T, Hattori H, Zenimaru Y, Suzuki J, Miyamori I, and Yamamoto TT (2004) The very low-density lipoprotein (VLDL) receptor: characterization and functions as a peripheral lipoprotein receptor, J. Atheroscler. Thromb 11, 200–208. [PubMed: 15356379]

(3). Jensen GA, Andersen OM, Bonvin AM, Bjerrum-Bohr I, Etzerodt M, Thogersen HC, O'Shea C, Poulsen FM, and Kragelund BB (2006) Binding site structure of one LRP-RAP complex: implications for a common ligand-receptor binding motif, J. Mol. Biol 362, 700–716. [PubMed: 16938309]

(4). Takahashi S (2017) Triglyceride rich lipoprotein -LPL-VLDL receptor and Lp(a)-VLDL receptor pathways for macrophage foam cell formation, J. Atheroscler. Thromb 24, 552–559. [PubMed: 28428482]

(5). Wyne KL, Pathak K, Seabra MC, and Hobbs HH (1996) Expression of the VLDL receptor in endothelial cells, Arterioscler. Thromb. Vasc. Biol 16, 407–415. [PubMed: 8630667]

(6). Yamamoto T, Takahashi S, Sakai J, and Kawarabayasi Y (1993) The very low density lipoprotein receptor. A second lipoprotein receptor that may mediate uptake of fatty acids into muscle and fat cells, Trends Cardiovasc. Med 3, 144–148. [PubMed: 21244941]

(7). Tacken PJ, Teusink B, Jong MC, Harats D, Havekes LM, van Dijk KW, and Hofker MH (2000) LDL receptor deficiency unmasks altered VLDL triglyceride metabolism in VLDL receptor transgenic and knockout mice, J. Lipid. Res 41, 2055–2062. [PubMed: 11108739]

(8). Takahashi S, Sakai J, Fujino T, Miyamori I, and Yamamoto TT (2003) The very low density lipoprotein (VLDL) receptor--a peripheral lipoprotein receptor for remnant lipoproteins into fatty acid active tissues, Mol. Cell. Biochem 248, 121–127. [PubMed: 12870663]

(9). D'Arcangelo G, Homayouni R, Keshvara L, Rice DS, Sheldon M, and Curran T (1999) Reelin is a ligand for lipoprotein receptors, Neuron 24, 471–479. [PubMed: 10571240]

(10). Battey FD, Gafvels ME, FitzGerald DJ, Argraves WS, Chappell DA, Strauss JF 3rd, and Strickland DK (1994) The 39-kDa receptor-associated protein regulates ligand binding by the very low density lipoprotein receptor, J. Biol. Chem 269, 23268–23273. [PubMed: 8083232]

(11). Mikhailenko I, Krylov D, Argraves KM, Roberts DD, Liau G, and Strickland DK (1997) Cellular internalization and degradation of thrombospondin-1 is mediated by the amino-terminal heparin binding domain (HBD). High affinity interaction of dimeric HBD with the low density lipoprotein receptor-related protein, J. Biol. Chem 272, 6784–6791. [PubMed: 9045712]

(12). Ujino S, Nishitsuji H, Hishiki T, Sugiyama K, Takaku H, and Shimotohno K (2016) Hepatitis C virus utilizes VLDLR as a novel entry pathway, Proc. Natl. Acad. Sci. U S A 113, 188–193. [PubMed: 26699506]

(13). Verdaguer N, Fita I, Reithmayer M, Moser R, and Blaas D (2004) X-ray structure of a minor group human rhinovirus bound to a fragment of its cellular receptor protein, Nat. Struct. Mol. Biol 11, 429–434. [PubMed: 15064754]

(14). Argraves KM, Battey FD, MacCalman CD, McCrae KR, Gafvels M, Kozarsky KF, Chappell DA, Strauss JF 3rd, and Strickland DK (1995) The very low density lipoprotein receptor mediates the cellular catabolism of lipoprotein lipase and urokinase-plasminogen activator inhibitor type I complexes, J. Biol. Chem 270, 26550–26557. [PubMed: 7592875]

(15). Heegaard CW, Simonsen AC, Oka K, Kjoller L, Christensen A, Madsen B, Ellgaard L, Chan L, and Andreasen PA (1995) Very low density lipoprotein receptor binds and mediates endocytosis of urokinase-type plasminogen activator-type-1 plasminogen activator inhibitor complex, J. Biol. Chem 270, 20855–20861. [PubMed: 7657671]

(16). Kasza A, Petersen HH, Heegaard CW, Oka K, Christensen A, Dubin A, Chan L, and Andreasen PA (1997) Specificity of serine proteinase/serpin complex binding to very-low-density lipoprotein receptor and a_2-macroglobulin receptor/low-density-lipoprotein-receptor-related protein, Eur. J. Biochem 248, 270–281. [PubMed: 9346278]

(17). Trommsdorff M, Gotthardt M, Hiesberger T, Shelton J, Stockinger W, Nimpf J, Hammer RE, Richardson JA, and Herz J (1999) Reeler/Disabled-like disruption of neuronal migration in knockout mice lacking the VLDL receptor and ApoE receptor 2, Cell 97, 689–701. [PubMed: 10380922]

(18). Hiesberger T, Trommsdorff M, Howell BW, Goffinet A, Mumby MC, Cooper JA, and Herz J (1999) Direct binding of Reelin to VLDL receptor and ApoE receptor 2 induces tyrosine phosphorylation of disabled-1 and modulates tau phosphorylation, Neuron 24, 481–489. [PubMed: 10571241]

(19). Hembrough TA, Ruiz JF, Swerdlow BM, Swartz GM, Hammers HJ, Zhang L, Plum SM, Williams MS, Strickland DK, and Pribluda VS (2004) Identification and characterization of a very low density lipoprotein receptor-binding peptide from tissue factor pathway inhibitor that has antitumor and antiangiogenic activity, Blood 103, 3374–3380. [PubMed: 14739228]

(20). Yakovlev S, Mikhailenko I, Cao C, Zhang L, Strickland DK, and Medved L (2012) Identification of VLDLR as a novel endothelial cell receptor for fibrin that modulates fibrin-dependent transendothelial migration of leukocytes, Blood 119, 637–644. [PubMed: 22096238]

(21). Yakovlev S, Belkin AM, Chen L, Cao C, Zhang L, Strickland DK, and Medved L (2016) Anti-VLDL receptor monoclonal antibodies inhibit fibrin-VLDL receptor interaction and reduce fibrin-dependent leukocyte transmigration, Thromb. Haemost 116, 1122–1130. [PubMed: 27580629]

(22). Yakovlev S, and Medved L (2015) Interaction of fibrin with the very low density lipoprotein receptor: further characterization and localization of the fibrin-binding site, Biochemistry 54, 4751–4761. [PubMed: 26153297]

(23). Wittekind M, and Mueller L (1993) Hncacb, a high-sensitivity 3d NMR experiment to correlate amide-proton and nitrogen resonances with the alpha-carbon and beta-carbon resonances in proteins, J. Magn. Reson. Ser. B 101, 201–205.

(24). Grzesiek S, and Bax A (1992) Correlating backbone amide and side-chain resonances in larger proteins by multiple relayed triple resonance NMR, J Am Chem Soc 114, 6291–6293.

(25). Grzesiek S, and Bax A (1992) Improved 3d triple-resonance NMR techniques applied to a 31-Kda protein, J. Magn. Reson 96, 432–440.

(26). Kay LE, Xu GY, and Yamazaki T (1994) Enhanced-sensitivity triple-resonance spectroscopy with minimal H_2O saturation, J. Magn. Reson. Ser. A 109, 129–133.

(27). Zwahlen C, Legault P, Vincent SJF, Greenblatt J, Konrat R, and Kay LE (1997) Methods for measurement of intermolecular NOEs by multinuclear NMR spectroscopy: Application to a bacteriophage lambda N-peptide/boxB RNA complex, J. Am. Chem. Soc 119, 6711–6721.

(28). Yang D, Zheng Y, Liu D, and Wyss DF (2004) Sequence-specific assignments of methyl groups in high-molecular weight proteins, J. Am. Chem. Soc, 126, 3710–3711. [PubMed: 15038713]

(29). Bax A, and Grzesiek S (1993) Methodological advances in protein NMR, Accounts. Chem. Res 26, 131–138.

(30). Clore GM, Kay LE, Bax A, and Gronenborn AM (1991) 4-Dimensional C-13/C-13-edited nuclear Overhauser enhancement spectroscopy of a protein in solution - application to Interleukin 1-beta, Biochemistry 30, 12–18. [PubMed: 1988012]

(31). Delaglio F, Grzesiek S, Vuister GW, Zhu G, Pfeifer J, and Bax A (1995) NMRPipe: a multidimensional spectral processing system based on UNIX pipes, J. Biomol. NMR 6, 277–293. [PubMed: 8520220]

(32). Vranken WF, Boucher W, Stevens TJ, Fogh RH, Pajon A, Llinas M, Ulrich EL, Markley JL, Ionides J, and Laue ED (2005) The CCPN data model for NMR spectroscopy: development of a software pipeline, Proteins 59, 687–696. [PubMed: 15815974]

(33). Garrett DS, Powers R, Gronenborn AM, and Clore GM (1991) a common-sense approach to peak picking in 2-dimensional, 3-dimensional, and 4-dimensional spectra using automatic computer-analysis of contour diagrams, J. Magn. Reson 95, 214–220.

(34). Bax A, Kontaxis G, and Tjandra N (2001) Dipolar couplings in macromolecular structure determination, Method Enzymol. 339, 127–174.

(35). Tjandra N, and Bax A (1997) Direct measurement of distances and angles in biomolecules by NMR in a dilute liquid crystalline medium, Science 278, 1697–1697.

(36). Hansen MR, Mueller L, and Pardi A (1998) Tunable alignment of macromolecules by filamentous phage yields dipolar coupling interactions, Nat. Struct. Biol 5, 1065–1074. [PubMed: 9846877]

(37). Ottiger M, Delaglio F, and Bax A (1998) Measurement of J and dipolar couplings from simplified two-dimensional NMR spectra, J. Magn. Reson 131, 373–378. [PubMed: 9571116]

(38). Shen Y, and Bax A (2013) Protein backbone and sidechain torsion angles predicted from NMR chemical shifts using artificial neural networks, J. Biomol. NMR 56, 227–241. [PubMed: 23728592]

(39). Schwieters CD, Kuszewski JJ, Tjandra N, and Clore GM (2003) The Xplor-NIH NMR molecular structure determination package, J. Magn. Reson 160, 65–73. [PubMed: 12565051]

(40). Schwieters CD, Kuszewski JJ, and Clore GM (2006) Using Xplor-NIH for NMR molecular structure determination, Prog. Nucl. Mag. Res. Sp 48, 47–62.

(41). Koradi R, Billeter M, and Wuthrich K (1996) MOLMOL: a program for display and analysis of macromolecular structures, J. Mol. Graph 14, 51–5, 29–32. [PubMed: 8744573]

(42). Wishart DS, and Sykes BD (1994) The ^{13}C chemical-shift index: a simple method for the identification of protein secondary structure using ^{13}C chemical-shift data, J. Biomol. NMR 4, 171–180. [PubMed: 8019132]

(43). Lipari G, and Szabo A (1982) Model-Free approach to the interpretation of nuclear magnetic-resonance relaxation in macromolecules .1. Theory and range of validity, J. Am. Chem. Soc 104, 4546–4559.

(44). Fass D, Blacklow S, Kim PS, and Berger JM (1997) Molecular basis of familial hypercholesterolaemia from structure of LDL receptor module, Nature 388, 691–693. [PubMed: 9262405]

(45). Yakovlev S, and Medved L (2017) Interaction of fibrin with the very low-density lipoprotein (VLDL) receptor: further characterization and localization of the VLDL receptor-binding site in fibrin bN-domains, Biochemistry 56, 2518–2528. [PubMed: 28437098]

(46). Maciejewski M, Tjandra N, and Barlow PN (2011) Estimation of interdomain flexibility of N-terminus of factor H using residual dipolar couplings, Biochemistry 50, 8138–8149. [PubMed: 21793561]

(47). Querol-Audi J, Konecsni T, Pous J, Carugo O, Fita I, Verdaguer N, and Blaas D (2009) Minor group human rhinovirus-receptor interactions: geometry of multimodular attachment and basis of recognition, FEBS. Lett 583, 235–240. [PubMed: 19073182]

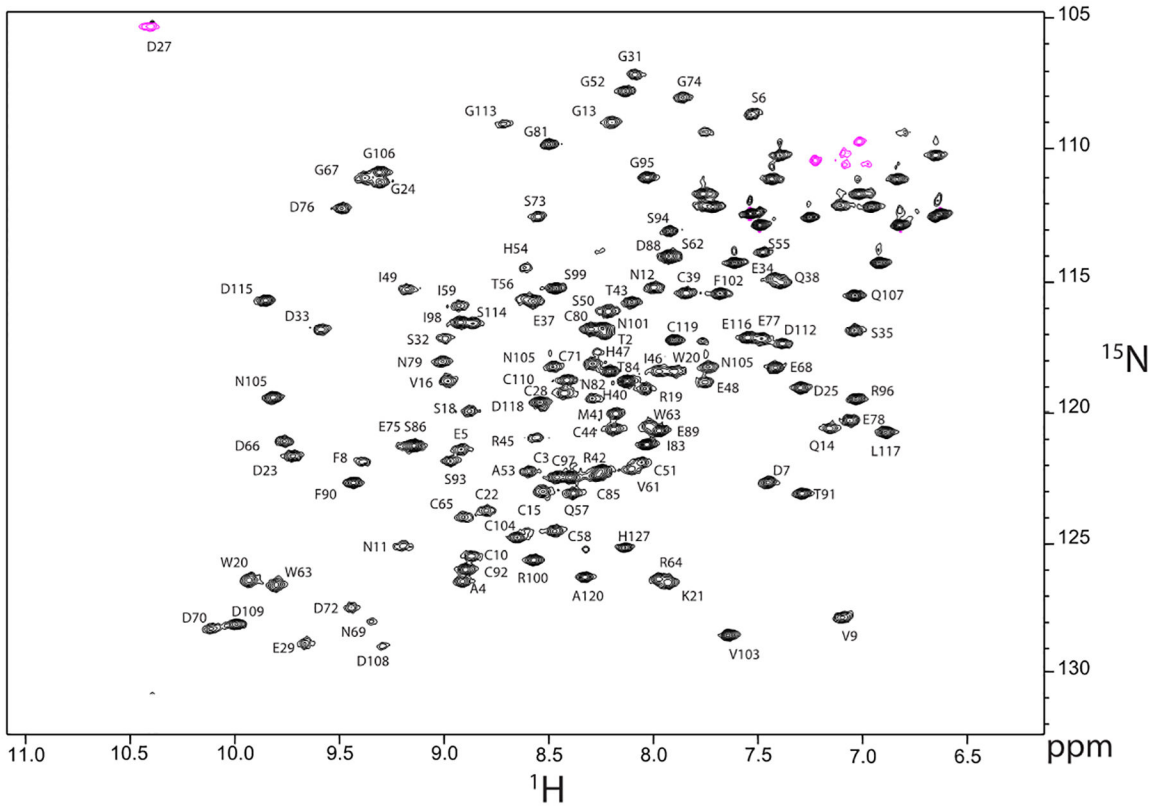

Figure 1.

Two-dimensional ^{1}H,^{15}N HSQC spectrum of the VLDLR(2–4) fragment shown with the backbone assignment. The negative intensities corresponding to folded resonances of Arg side chains and NH of D27 are shown in pink.

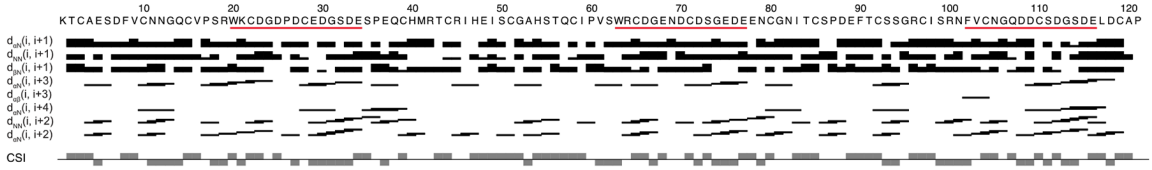

Figure 2.

Summary of the sequential and medium range NOEs involving the H_N, H_α, and H_β protons. The chemical shift index (CSI)[42] is shown at the bottom. Residues in the calcium-binding loops are underlined in red.

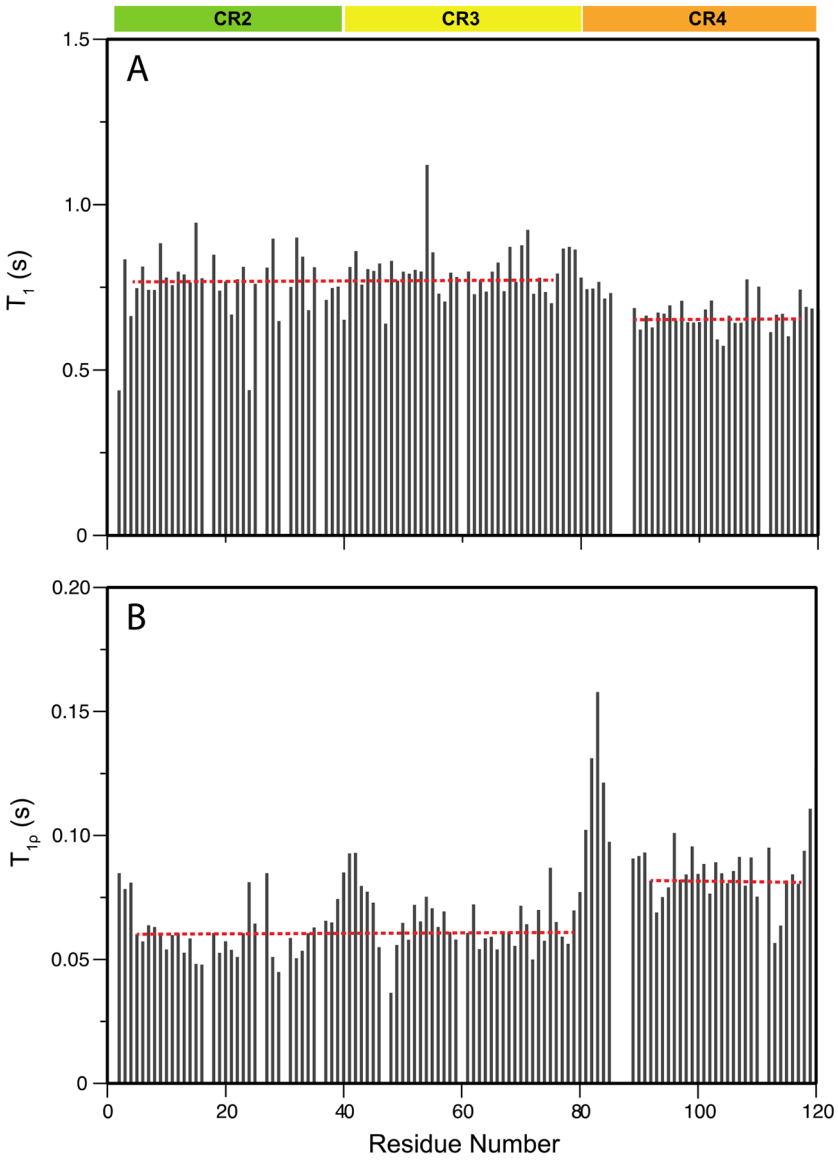

Figure 3.

Backbone dynamics of the VLDLR(2–4) fragment. Panels (A) and (B) show the experimental values of ^{15}N T_1 and $T_{1\rho}$, respectively, for VLDLR(2–4). Regions belonging to different CR domains are indicated at the top of the panel in bars with three different colors, green, yellow, and orange. The horizontal dotted red lines show the average T_1 and $T_{1\rho}$ values obtained by averaging the experimental data over all residues in CR2–3 and CR4. Residues in highly flexible loops are excluded from the calculation of the average values.

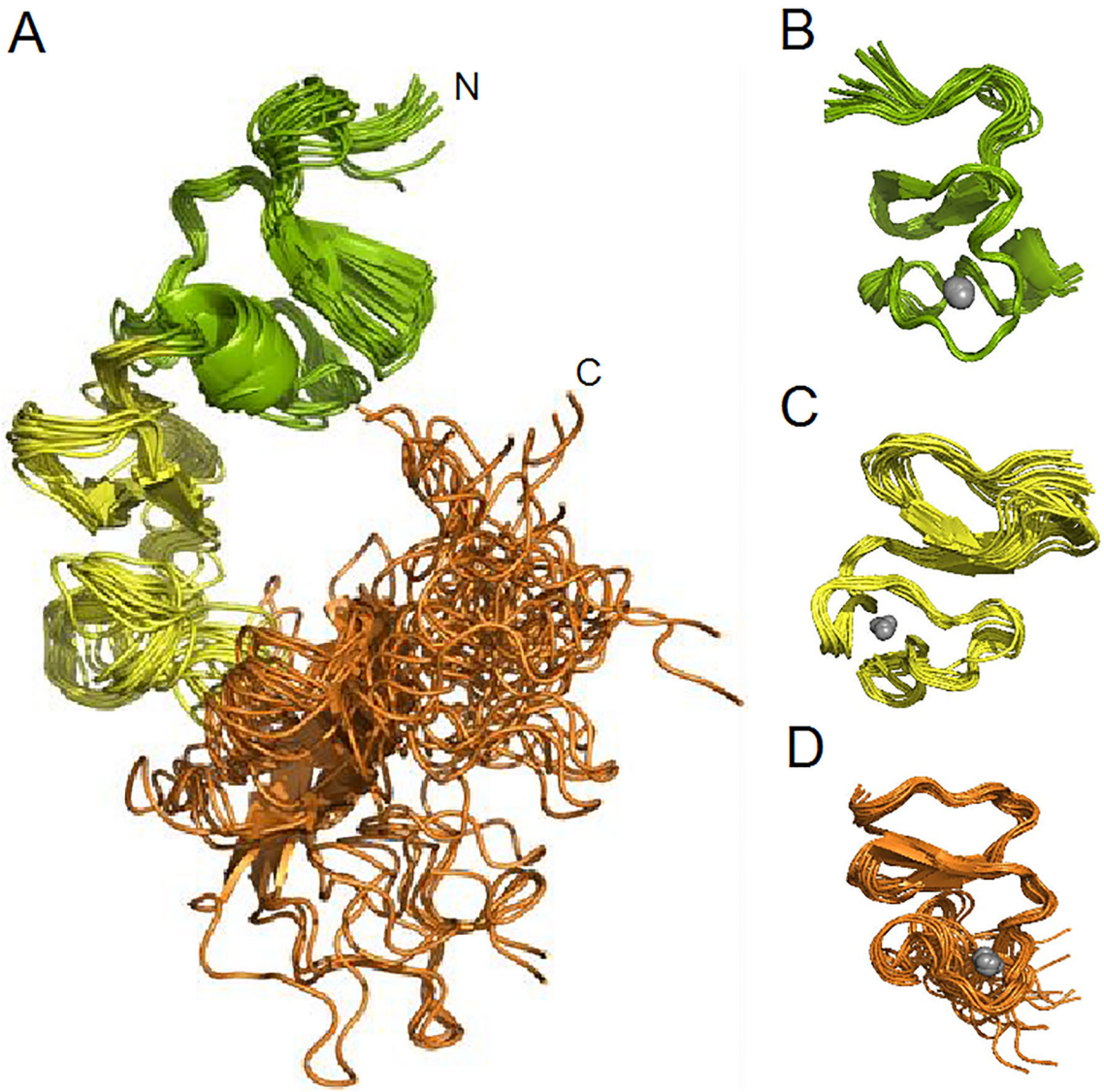

Figure 4.

(A) Superposition of an ensemble of 20 lowest energy structures of the VLDLR(2–4) fragment with CR2 domain in green, CR3 in yellow, and CR4 in orange. The superposition was calculated by least square fit the backbone atoms of CR2–3. Superposition of the CR2 domain (residues 5–38) is shown in (B), CR3 (residues 43–74) in (C), and CR4 (residues 80–116) in (D).

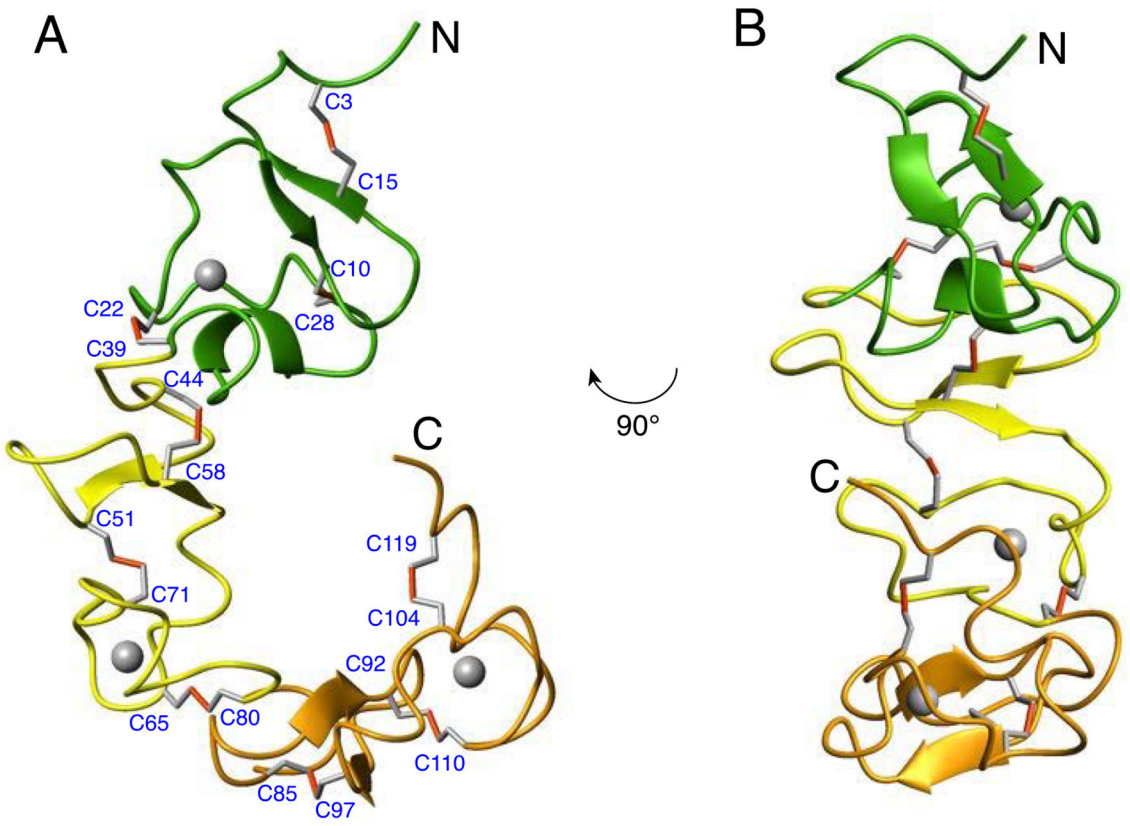

Figure 5.

(A) ribbon representation of the lowest energy structure of the VLDLR(2–4) fragment with CR2, CR3, and CR4 domains colored green, yellow, and orange, respectively; Ca^{2+} ions are shown as grey spheres. The structure depicts very short stretches of regular secondary structures and longer loop regions which are stabilized by extensive network of nine disulfide bonds. The pairing of cysteine residues are indicated with the disulfide bonds represented in red. (B) Another view of the ribbon representation of the VLDLR(2–4) structure highlighting the relative orientation of the antiparallel β-sheet in CR2 domain (green) which is almost 90° from CR3 (yellow).

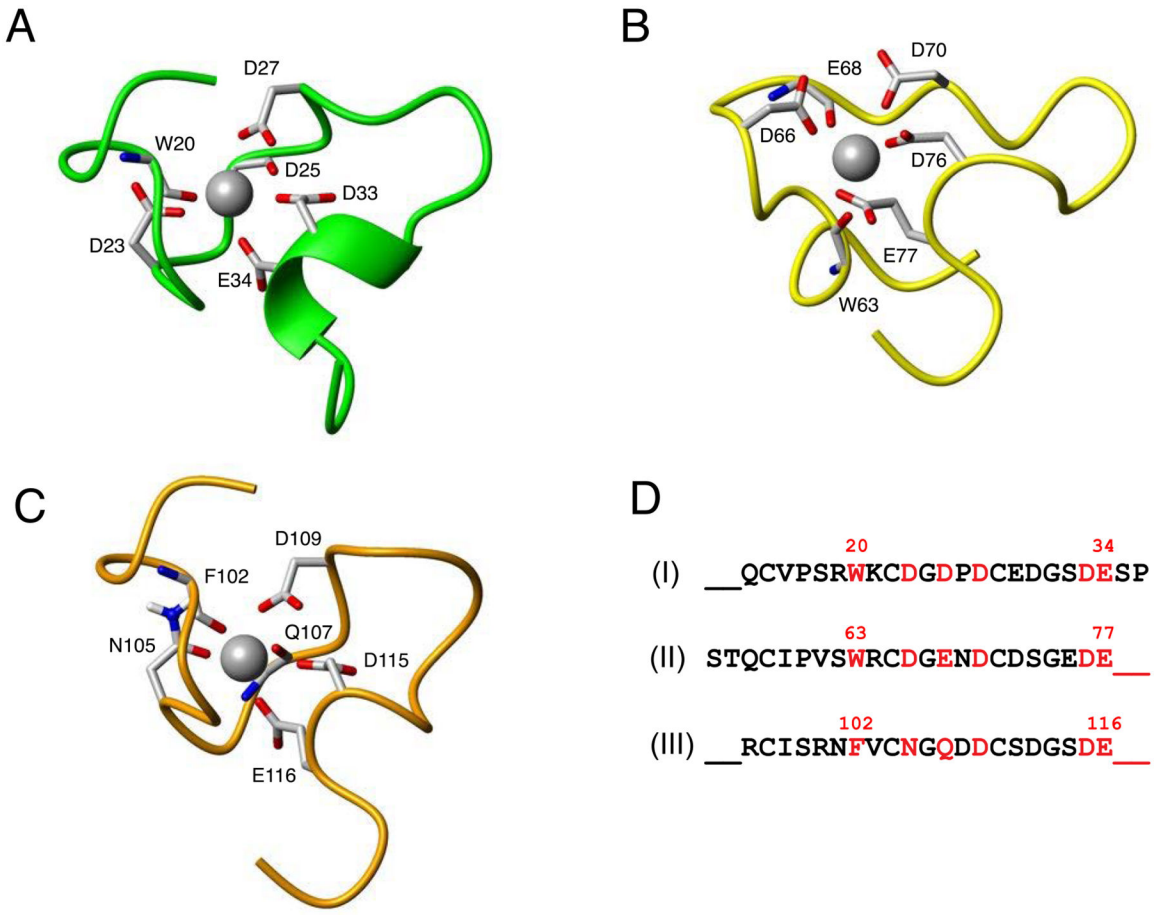

Figure 6.

Calcium-binding pockets of the VLDLR(2–4) fragment. Ligands for Ca^{2+} binding in CR2, CR3, and CR4 domains are shown in (A), (B), and (C), respectively. Ca^{2+} ions are shown as grey spheres, while side chains of the residues that co-ordinate with these ions are shown in sticks. The structures of the three calcium-binding loops are shown by superimposing them on the last three residues (S32-E34, E75-E77, S114-E116) so that they have the same relative orientation. (D) Sequence alignment of the three Ca^{2+}-binding regions of CR2, CR3, and CR4 domains (I, II, and III, respectively) with the ligand residues colored in red and the 2-residue inserts in CR2 and CR3 shown at the end and the beginning of their sequences, respectively.

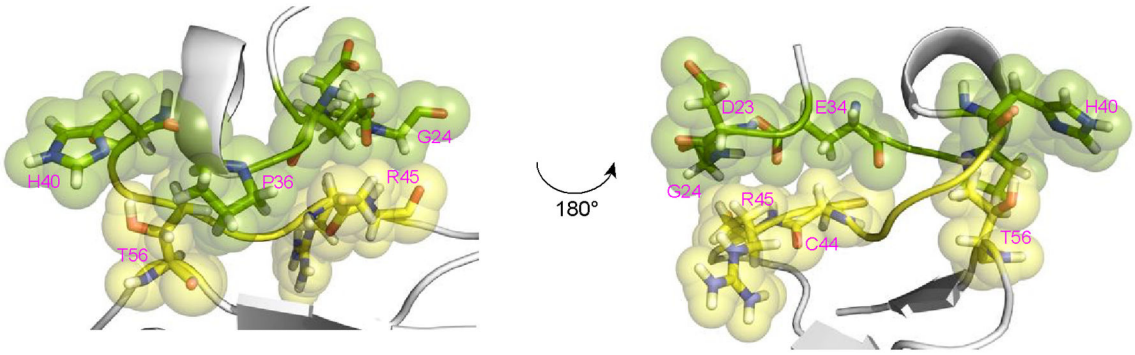

Figure 7.

Interdomain packing in the VLDLR(2–4) fragment. Residues involved in stabilizing CR2-CR3 domain packing are highlighted in the left panel. The right panel is 180° rotated view of the left panel. Residues belonging to CR2 and CR3 are shown in green and yellow spheres, respectively, and are labeled in magenta. Insert residues P36 and T56 are included.

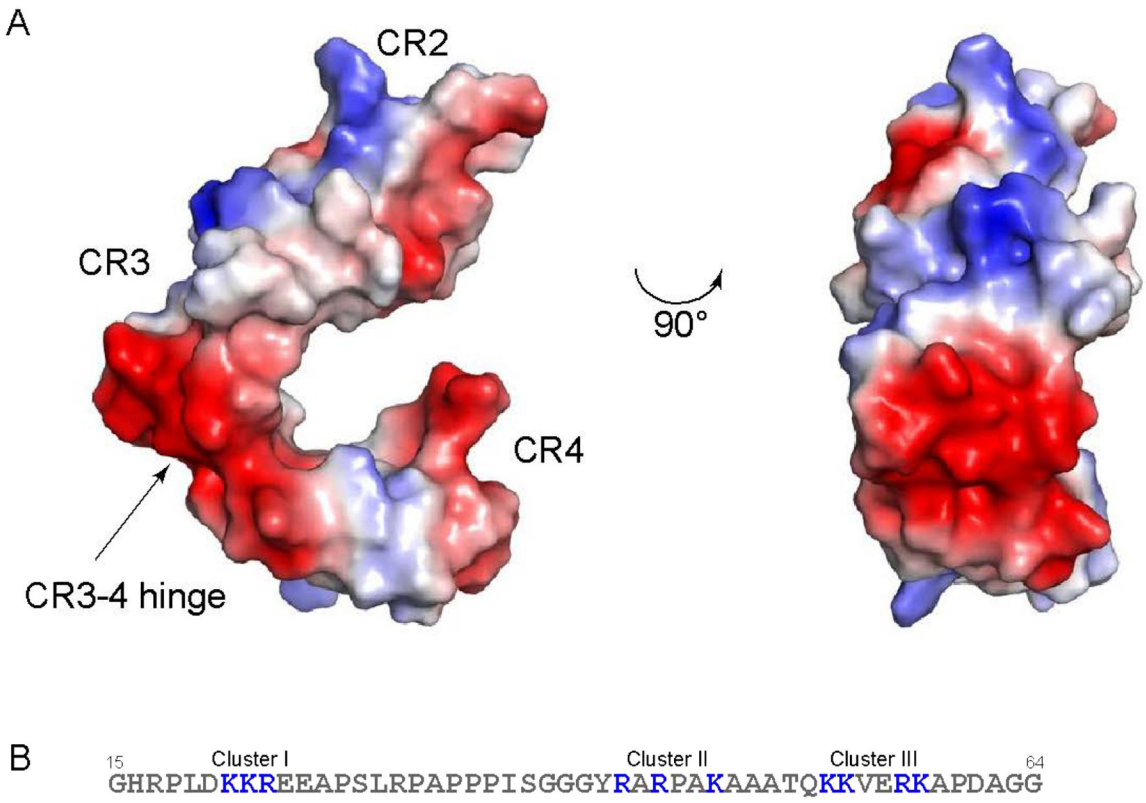

Figure 8.

(A) Electrostatic surface potential of the VLDLR(2–4) fragment. The surface potential was calculated using the program PyMOL. Positively charged residues are shown in blue, while negatively charged residues are in red. The different CR domains and the hinge between CR3 and CR4 are indicated. The right view is 90° rotated with respect to the left panel. (B) βN-domain sequence (amino acid residues β15–64) with the positively charged clusters highlighted in blue.

Table 1:

Structural statistics of an ensemble of 20 lowest energy structure of VLDLR (PDB ID: 6BYV), derived from XPLOR and PSVS 1.5.

Distance restraints (Å)			
NOE (1606)[a]			0.21 ± 0.01
Intraresidue NOE (|i-j| = 0) (303)			0.22 ± 0.01
Sequential NOE (|i-j| = 1) (465)			0.19 ± 0.01
Medium range NOE (2 ≤ |i-j| ≤ 5) (468)			0.25 ± 0.02
Longrange NOE (|i-j| ≥ 6) (370)			0.26 ± 0.03
H-Bonds (9 × 2)			0.25 ± 0.11
Dihedral angle restraints (°)			
ϕ and ψ (106 × 2)			4.10 ± 0.47
Residual Dipolar Coupling (104)	R-factor	D_a	R_h
5–80	21.67 ± 1.41	−4.43 ± 0.03	0.55 ± 0.00
93–118	19.62 ± 4.27	5.00 ± 0.03	0.40 ± 0.00
Deviations from idealized covalent geometry			
Bond (Å) (1698)			0.01 ± 0.00
Angle (°) (3014)			1.16 ± 0.05
Improper (°) (877)			1.15 ± 0.07
Coordinate precision RMSD (Å)	All backbone atoms (Å)		All heavy atoms
5–38	0.64 ± 0.27		0.98 ± 0.28
43–74	0.65 ± 0.27		0.95 ± 0.27
80–116	1.94 ± 1.11		2.07 ± 1.08
All ordered[b]	2.85 ± 1.34		2.98 ± 1.29
Ramachandran plot			
Residues in most favored regions			69.7%
Residues in additional allowed regions			27.8%
Residues in generously allowed regions			2.4%
Residues in disallowed regions			0.1%

[a] Total number of restraints and

[b] Residues in regular secondary structure: 5–38, 43–74, 80–116 (80–98 and 102–116) and Calculated using PSVS/Procheck